A Feasibility Study on Flapping Wing Actuation using Dielectric Elastomers

Srinivasan G Ram[1,3], Paul George[2], Jaideep Sharma[2], Ramesh Gupta[1] and Dineshkumar Harursampath[3]

[1] Department of Mechanical Engineering, Shiv Nadar University, Greater Noida, India
[2] Department of Electrical Engineering, Shiv Nadar University, Greater Noida, India
[3] Department of Aerospace Engineering, Indian Institute of Science, Bengaluru, India

E-mail: rameshgupta.iisc@gmail.com

ABSTRACT

Introduction of smart materials as actuators in flapping wing micro aerial vehicles (MAVs) eliminates the need for the traditional rotary power delivery mechanisms, allowing for lighter, smaller and more energy efficient designs. General kinematics of insect flight is investigated to relate the independent variable wing length to two dependent variables wingbeat frequency and stroke amplitude, to establish a benchmark of characteristics the smart material must possess. Dielectric Elastomers due to their high actuation strain, high actuation speed, low density, compliant nature and silent operation were evaluated to be suitable for flapping wing actuation. Through an experimental reference design study, corresponding finite element validation and extrapolation of the model to a unimorph bender actuator representative of an insect wing, a path is laid to achieving the kinematic parameters required for flight. Further modelling and analysis of the high voltage custom waveform generator and sensing circuit used in the experiments is done using a SPICE simulator.

Keywords: Flapping Wing MAVs, Dielectric Elastomers, Smart Materials, Unimorph Actuators

NOMENCLATURE

C(V)	capacitance as a function of voltage
C10, C20, C30	Yeoh hyperelastic model material constants
C_o	capacitance prior to deformation
Cs	high voltage bypass capacitor
E	electric field
P	maxwell stress
Ri	leakage resistance of the elastomer
Ro	output impedance of the secondary transformer
s(V)	straining of the active region as a function of voltage
V	applied voltage
V_{in}	stepped down voltage
V_{Out}	high voltage output
z	film thickness
β	stroke plane angle
η	wingbeat frequency
ε	relative dielectric constant
ε_0	permittivity of free space ($8.85e^{-12}$ F/m)
φ	sweep angle or stroke angle
ψ	pitch angle
ϕ	stroke amplitude
θ	stroke deviation angle

1.0 INTRODUCTION

Unmanned Aerial Vehicle (UAV) research has been one of the more active fields in the twenty first century with new and innovative designs coming out every year. Applications for these UAVs are vast both in the military and commercial sectors. Over the past two decades the trend has been towards the development of smaller and smaller UAVs [1]. Two major classes of UAVs have emerged from this trend: Micro Aerial Vehicles (MAVs) and Nano Aerial Vehicles (NAVs). According to DARPA, UAVs with a maximum dimension of 15 cm and weight 200 g may be classified as MAVs, whereas UAVs with dimensions much less than 15 cm and weight less than 20 g may be classified as NAVs [2]. A number of fixed wing aircrafts and multi-rotors have been designed at the micro scale, but researchers are faced with a number of unique challenges when moving to the nano scale, given the sensitive Reynolds number regime these vehicles have to operate in.

Nature has produced numerous flying machines in the form of insects that have perfected flying in this low Reynolds number regime by evolution over millions of years. Research has established that at this scale, aerial vehicles adopting flapping wings rather than conventional propeller systems presents a number of advantages in terms of lift generation, hovering capability, manoeuvrability, power requirement, silent operation and high payload [3-6]. Studying the aerodynamics and kinematics behind the flight capabilities of insects helps in solving some of the unique challenges thrown up by the low Reynolds number regime. Insect wing kinematics study reveals that flapping involves simultaneous bending and twisting action of the wings to generate the aerodynamic forces required for flight [7]. Conventional flapping wing mechanisms rely on either pneumatic or electric motor driven flapping actuators leading to heavy, bulky and complex systems. This makes it difficult to mimic insect wing kinematics.

Development in the field of smart materials such as piezoelectric fibre composites and electro active polymers (EAPs) have proven their potential to serve as actuators. Introduction of these materials into the flapping wing mechanisms eliminates the need for conventional actuators and transmission systems [3], [6-7]. They also open up a possibility of achieving the efficiency, manoeuvrability and autonomous operation found in nature, to which conventional power delivery mechanisms have always been a limiting factor. Hence arises a need to examine the current state of the art of these smart materials and evaluate if they can serve as flapping wing actuators.

The present work aims to investigate the underlying motions that generate lift in insects and the potential of available smart materials for flapping wing actuation. Through an experimental reference design study, the influence of physical parameters such the material, actuation frequency and stimulus shapes on the strain produced in dielectric elastomers is investigated. A finite element model is developed based on the experimental observation to model a unimorph bender actuator analogous to a flapping wing of an insect. Further the high voltage generator and sensing circuit used in the experiments, along with the dielectric elastomer is modelled and analysed using a SPICE simulator

2.0 FLAPPING WING ACTUATION

2.1 BIOMIMETIC STUDY OF KINEMATICS

A number of studies have been carried out to analyse the underlying motions that generate the required lift forces in insects. Most of these studies follow the conventions and terminologies laid out by C.P Ellington's work on the aerodynamics of hovering insect flight and this paper adopts the same [10]. Insect flight in general involves 3 degrees of freedom (two components of translation and one component of rotation): the main flapping motion, out of plane flapping motion and active wing rotation. These motions are engaged in a set sequence by insects, inducing minor variations to carry out the various manoeuvres required during flight. These motions can be broken down to four sequential phases as listed below [11]:

a) Down-stroke – Forwards and downwards
b) Stroke Reversal – Backwards rotation (Supination)
c) Up-stroke – Backwards and upwards
d) Stroke Reversal – Forwards rotation (Pronation)

In order to compare the finer motions of different species of insects a number of parameters are tracked. The critical ones are listed below [10-11]:

a) Stroke plane angle, β: Angle of inclination of the stroke plane – measured relative to the horizontal about which the main flapping motion takes place.
b) Sweep angle or stroke angle, φ: Tracks the main flapping motion of the wing, measured about an axis perpendicular to the stroke plane.
c) Pitch angle, ψ: Tracks the rotation/ twisting motion of the wing.
d) Stroke deviation angle, θ: Describes the out of plane flapping motion. The wingtip trajectory can be mapped using a combination of sweep angle and stroke deviation angle.
e) Stroke amplitude, ϕ: Range of the sweep angle φ over an entire wingbeat. Increase in ϕ leads to an increase in aerodynamic forces generated.
f) Wingbeat frequency, η: Number of pronation's per second. Most insects tend to match their wingbeat frequencies with the resonant frequency of their wings. Increase in η also leads to an increase in the aerodynamic forces generated.

2.2 CASE STUDIES

A truly biomimetic approach replicating all aspects of insect flight to design a flapping wing MAV would neither be optimal nor feasible. This is augmented by the fact that different insect species of different sizes have evolved to have different kinematic parameters for flight. Instead it would be more prudent to isolate some broader kinematic parameters which will help in narrowing down on an optimal actuator material. Some of these parameters have been compiled in **Table 1** for a range of species [12–18].

Table 1: **Key kinematic parameters of insect flight**

Order	Species	Wing Length (mm)	Wingbeat Frequency (Hz)	Stroke Amplitude (°)
Dipterans	Vegetable Leaf-miner	1.4	265	180
	Fruit Fly	3	240	150
	Drone Fly	11	170	110
Hymenopterans	Honey Bee	9.7	226	86
	Bumble Bee	14	155	115
Lepidopterans	Hawk Moth	48.5	25	105
Odonatans	Dragonfly	40	32	70

Given that the ultimate goal is to generate the unsteady aerodynamic forces needed for flying, replicating these key kinematic parameters will give a baseline to start. It is evident from **Table 1** that the wing kinematics of insects have considerable variations from species to species. Hence some generalized parameters are arrived at for larger insect species as they are the least demanding in terms of wingbeat frequency. These generalized parameters will serve as goalposts when smart materials are evaluated in sections to follow.

- Target wing length: 50 mm
- Target wingbeat frequency: 30 Hz
- Target stroke amplitude: 70°

3.0 SMART MATERIALS

3.1 MATERIAL SELECTION

Smart materials also referred to as intelligent materials are engineered to have one or more properties that can be modified using external stimuli such as mechanical stress, temperature and electric fields among others [21]. For flapping wing actuation, the most suitable materials would be ones that output linear mechanical strain when subject to electrical field stimulus. This narrows down the materials of interest to piezoelectric fibre composites (PFCs) and electro active polymers (EAPs). Further electro active polymers can be categorized into Ionic EAPs and Electronic EAPs based on their activation mechanisms. Ionic Polymer Metal Composites(IPMC) and Dielectric Elastomers (DE) are the leading materials from each category respectively [22]. Some key material and actuation properties of each of these materials has been compiled in **Table 2** [11], [20-29].

Table 2: **Key material and actuation properties of PFCs & EAPs**

Properties	Macro Fibre Composites	Ionic Polymer Metal Composites	Dielectric Elastomers
Actuation Voltage	High (2 kV)	Low (4-7 V)	Very high (3-7 kV)
Motion	Fibre elongation	Bending	Elastomer elongation
Density	5.44 g/cm^3	1 – 2.5 g/cm^3	1 – 1.2 g/cm^3
Strain	0.15 %	NA	60 % - 380 %
Actuation Force	High	Low	High
Efficiency	16 %	NA	60 % - 90 %
Speed of Actuation	Fast	Slow	Medium
Representative Geometries	Linear extender, bimorph, unimorph	Bending cantilevers	Linear extender

From the table, it can be observed that dielectric elastomers exhibit superiority in terms of low density, high strain, high actuation force, reasonable efficiency and actuation speeds. It also permits good flexibility in design as the elastomer's linear motion can be hijacked to produce a variety of configurations such as unimorphs, bimorphs, extenders, diaphragms, rolls and tubes to name a few [25]. Only drawback presented by dielectric elastomers is the requirement of a high voltage source to power the actuation. Given the progress made by electronics manufacturers in the recent years on ultra-miniature high voltage DC-DC converters this is no longer a major issue [32].

3.2 DIELECTRIC ELASTOMER

Dielectric elastomers are compliant variable capacitors, consisting of a thin elastomeric film coated on both sides with compliant electrodes. Upon application of an electric field across the electrodes, the electrostatic attraction between opposing charges on the compliant capacitor electrodes and the repulsion between like charges within the compliant electrodes generate stress on the elastomer causing it to contract in thickness and expand in area [31-32]. This is shown in **Figure 1**.

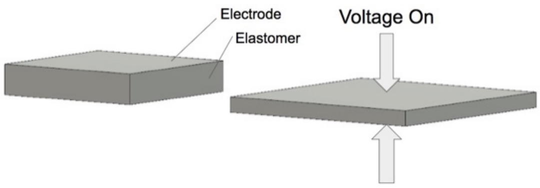

Figure 1: Dielectric elastomer actuation

Operating voltages can vary from 500 V to 10 kV depending on the strains required and the thickness of the elastomer. The area expansion that takes place upon voltage application can be readily measured if the films are pre-strained, as the non-active areas in tension surrounding the complaint electrodes pulls the active area while keeping it flat. Prior research indicates that the driving currents are extremely low, and power is only consumed when active electrode expansion takes place [35]. No power is consumed to hold and maintain the dielectric elastomer in a stable actuated state. Though in practice there may be small leakages through the dielectric, these are negligible.

The output stress, referred to as Maxwell stress varies quadratically with the electric field and can be summarized to the following expression:

$$P = \mathcal{E}\mathcal{E}_0 E^2 = \mathcal{E}\mathcal{E}_0 (V/z)^2 \qquad \ldots(1)$$

where, $\mathcal{E}$ is the relative dielectric constant, $\mathcal{E}_0$ is the permittivity of free space ($8.85e^{-12}$ F/m), E is the applied electric field, V is the applied voltage, and z is the film thickness [36].

A number of acrylic and silicone elastomer materials have been experimented with and both present their own pros and cons. One of the most popular ones is the commercially available 3M VHB 4905/10 acrylic elastomers. They have exhibited high efficiencies and good strain performance, with strains in excess of 380% for highly pre-strained films [37]. Silicone elastomers have lower viscoelasticity than acrylic elastomer and can hence be operated at higher frequencies with lower losses. Given that silicone elastomers are not readily available in the market and the fact that their lower dielectric constant will require higher actuation voltages, preference is given to acrylic elastomers for preliminary experimental studies.

4.0 EXPERIMENTAL MODEL

The schematic of the entire setup is shown in **Figure 2**. The following sections examine each block of the figure in detail.

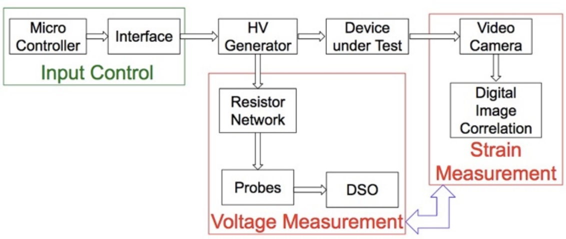

Figure 2: Experimental setup schematic

4.1 TEST SAMPLE SPECIFICATIONS

The sample preparation process begins with a circular stencil of 4 cm inner diameter and 5 cm outer diameter. This stencil is used to cut out 3M VHB 4910 [38] elastomer in a circular shape. This elastomer is stretched over the frame having an inner diameter of 11 cm and an outer diameter of 12 cm. The elastomer is securely bound to the frame using cable ties. Then small strips of copper tape is attached to both sides of the elastomer. Following this both sides of the elastomer are precisely coated with the compliant electrode, conductive carbon grease [39]. The region coated with carbon grease is refered to as the active region and amounts to 4 cm in diameter. The thickness of this coating is 0.08±0.01 mm. The capacitance of these samples are measured to be between 440-600 pF. The prestrain is three times the original diameter of the elastomer i.e at a ratio of 3:1. This ratio of prestrain is used as repeatablility in experimental results are quite good [40]. The thickness of the film was measured using a digimatic micrometer (Mitutoyo – Series 293) before (1 mm) and after (0.093±0.001 mm) prestraining. The sample is shown in **Figure 3** and the parameters listed above are kept constant throughout the experiments that follow.

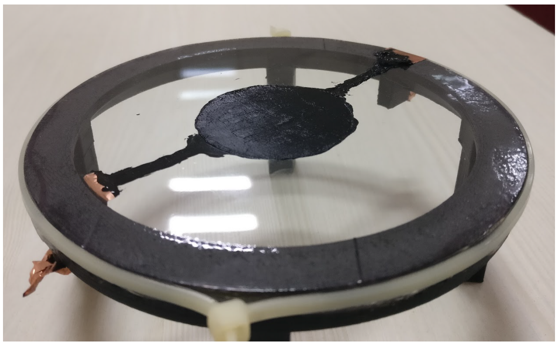

Figure 3: Dielectric elastomer test sample

4.2 HIGH VOLTAGE GENERATION AND CONTROL

The high voltage generator used to actuate the dielectric elastomer was procured off the shelf [41]. It is capable of maintaining a potential difference between 1000 V to 10 kV. The generator is powered by a 10 V DC input. The variable potentiometer integrated in the circuit can be used to vary the output of the generator. Using a Digital Storage Oscilloscope (DSO) it is determined that the wiper/output voltage of the potentiometer is between 0-1.4 V. The corresponding high voltage output is depicted in **Figure 4**.

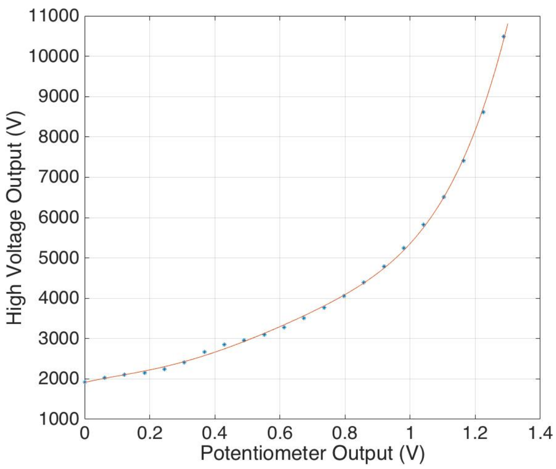

Figure 4. HV generator output with changing potentiometer output

It can be observed that the relation is fairly linear up to 6000 V, which is the upper limit for all experiments that follow. The variable potentiometer that is used to vary the output of the high voltage generator is replaced with a microcontroller and an interface as shown in **Figure 5.** Using this various actuation patterns in terms of both varying voltage and frequency can be programmed for the desired output patterns.

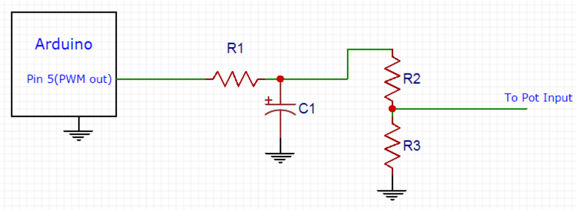

Figure 5. Microcontroller and interface

4.3 VOLTAGE MEASUREMENT

Though a relation between microcontroller input and high voltage generator output is available, a real-time measurement of the potential difference across the device under test is necessary. This measurement is done by first stepping down the voltage using a high impedance resistor network as shown in **Figure 6**.

$$V_{Out} = V_{in}*(R_1+R_2+R_3+R_4)/R_4 \qquad \text{...(2)}$$

Where, V_{Out} is the high voltage output and V_{in} is the stepped down voltage measured across R_4 using a DSO. R1, R2 are 100 MΩ resistors, R3 is a 10 MΩ resistor and R4 is an 810 kΩ resistor. All five capacitors have a voltage rating of 3 kV.

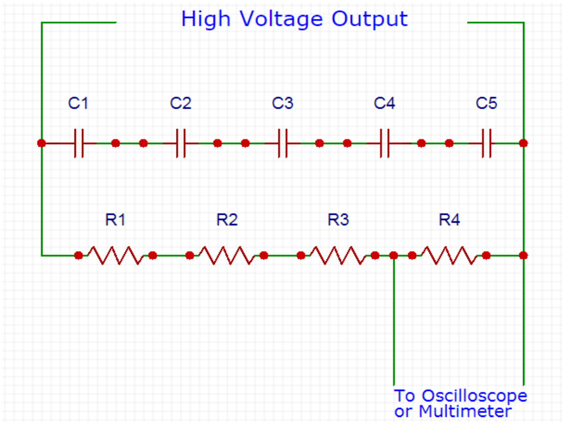

Figure 6. High impedance resistor network

A series of capacitors are also connected to this circuit to minimize the signal noise present in the output high voltage. Experimental data measured this way is exported as a CSV file to carry out post processing in MATLAB.

4.4 STRAIN MEASUREMENT

Given that the sample comprises of an elastomer with an adhesive surface and conductive grease, contact based strain measurement devices cannot be used. Non-contact strain measurement was done using a technique called Digital Image Correlation (DIC) [42]. DIC tracks the movement of pixels in a specified region of the video on a frame by frame basis. The active region of the sample was set as the region of interest using grid markers for the DIC process as shown in **Figure 7**.

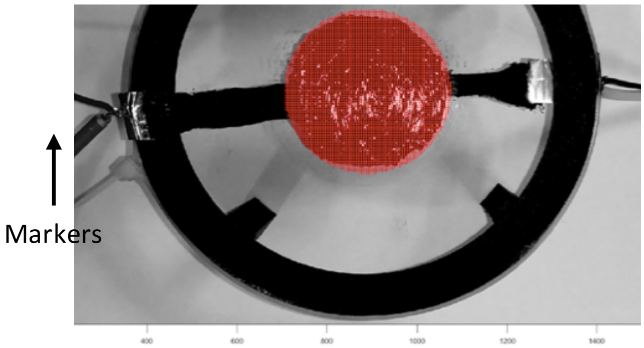

Figure 7. Grid markers

The grayscale video was recorded with a frame size of 1920×1080 at 30 fps, providing 30 frames worth of data for each second of recording.

5.0 COMPUTER MODELLING & SIMULATION

Finite element modelling of dielectric elastomers is carried out using a commercial engineering simulation software, ANSYS Parametric Design Language (APDL) [43]. The high voltage generator and sensing circuitry is modelled using LTspice, a high-performance simulation software, schematic capture and waveform viewer for analog circuits.

5.1 DISC ACTUATOR

The disc actuator is designed to serve as a finite element counterpart of the experimental model. In this regard a disc is designed with a diameter of 12 cm and thickness of 0.093 mm. Solid226 is the chosen element type, as it is capable of both static and transient electro-mechanical coupled field analysis and has structural capabilities to handle hyperelasticity and large strains [44]. Literature suggests Yeoh hyperelastic materials models once optimized to the electromechanical experimental values, are stable under high loads and can serve as a good benchmark for further experiments [38-39]. Strain data procured numerically is juxtaposed against the experimental data and an optimization process is carried out to reduce the error between the two. Viscoelastic effects are neglected, as the focus here is not on a cyclic charge-discharge study. The relative electrical permittivity value of 4.7 for VHB 4910 is supplied to the software in accordance with contemporary literature [40]. Mapped meshing is carried out on the 3D model using hexahedral-shaped elements.

A fixed constraint is applied to the curved surface area constraining all degrees of freedom, simulating the role of the frame and cable ties in the experimental sample. Further, movement in the normal direction is constrained at the bottom surface of the disc, replicating the role prestrain plays in the experimental samples. At the top and bottom surfaces of the disc for a region 4 cm in diameter, electrical loads are specified. The bottom region is set to ground and the top region is set to a variable voltage parameter. These electrode regions are indicated by the black region in **Figure 8**.

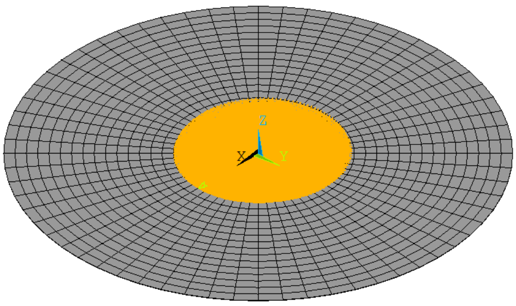

Figure 8. Disc actuator finite element model

The physical effects induced by carbon grease in the experimental model is ignored for the time being. The evaluation is carried out for voltage parameter values ranging between 1500 V to 5000 V.

5.2 UNIMORPH BENDER ACTUATOR

The bender actuator is designed keeping in mind the target wing length of 50 mm. Hence it comprises of two layers, the elastomer layer and the chosen substrate, polymethylsiloxane (PDMS). PDMS is preferred given the lower modulus of elasticity (kPa range) when compared with substrate options such as Mylar (GPa range) to aid in the bending motion. Both the elastomer and substrate have identical dimensions lengthwise (50 mm) and widthwise (12 mm). The thickness of the elastomer is as per the experimental observation, 0.093 mm. The thickness of the substrate is taken to be 0.12 mm. Solid226 is chosen as the element type for the elastomer, while a compatible solid185 is chosen for the electrically inactive substrate. The optimized hyperelastic material model is carried forward from the disc actuator for the elastomer. The material properties for the substrate is incorporated as is from relevant literature [47]. Mapped meshing is carried out for the entire model.

One end of the bender is constrained to emulate the fixed end of a cantilever beam. Further the movement in the lateral direction is constrained to accentuate the bending motion. At the top and bottom surfaces of the elastomer, ground and voltage loads are applied at a base region of length 30 mm, similar to the disc actuator setup. These regions are indicated in orange in **Figure 9**. The evaluation is carried out for multiple voltage loads to assess the bending.

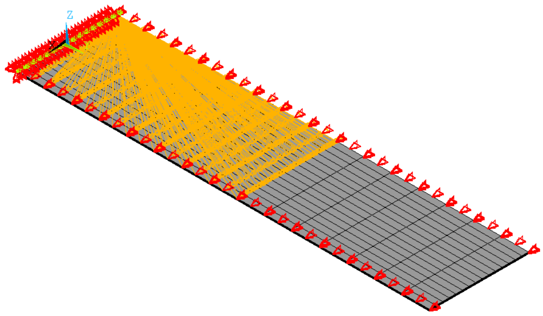

Figure 9. Unimorph bender actuator finite element model

5.3 HIGH VOLTAGE STIMULUS APPARATUS

The dielectric electric elastomer is a nonlinear charge storage device. The capacitance of the structure varies as the material deforms on voltage application. A programmable high voltage generator and sensing circuit was put together to simulate the prepared elastomer sample over a voltage range of 0 - 10KV DC with a peak output current of 5mA making it capable of delivering a maximum of 50W of power. The modelled circuit is shown in **Figure 10**.

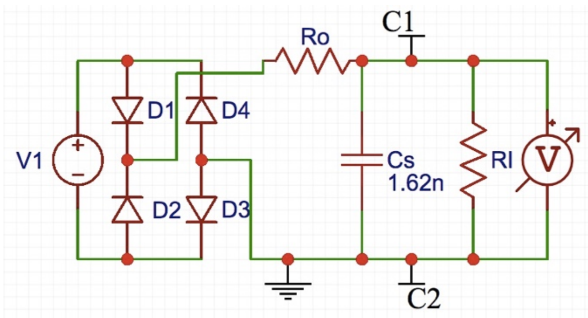

Figure 10. High voltage stimulus apparatus

The circuit was fitted with diodes to protect the generator and sensor against reverse current flows. A 1.62nF high voltage bypass capacitor(Cs) was added to minimise the generators output ripple, in replica to the experimental setup. Ro indicates the output impedance of the secondary transformer and Ri indicates the leakage resistance of the elastomer. A competent voltmeter was used to safely measure the voltage developed across the device. Terminals C1 and C2 represent the points across which the dielectric elastomer is connected.

The capacitance of the incompressible poly-acrylate elastomer is modelled as a relation between strain, potential difference and capacitance prior to the deformation as described by the expression below:

$$C(V) = C_o*(1+s(V))^4 \qquad \ldots(3)$$

Where, V is the potential difference across the device, C_o is capacitance prior to deformation and s(V) is the straining of the active region as a function of V.

6.0 RESULTS

6.1 STRAIN RESPONSE TO VOLTAGE

The first set of experiments performed on the sample is to gauge the strain response to increasing voltage. The microcontroller is programmed to increase the voltage in a stepwise fashion, in order to afford the elastomer time to reach a stable state. The data obtained through the DSO and the camera is processed as described in the sections above. This data is synchronised with respect to time based on additional audio and visual indicators setup during the experiment. This is repeated over several fresh samples to iron out any abnormalities that may arise due to material defects. The outcome of these experimental runs are accumulated and a 3rd order polynomial curve fitting is done to arrive at a reasonable prediction methodology for future experiments where either the operating voltage or observed strain value is known as shown in **Figure 11**.

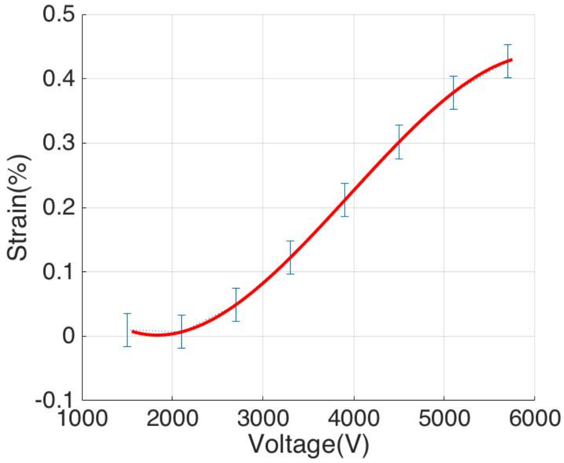

Figure 11. Strain response to increasing voltage, with error bars indicating standard deviation

The measurement range is restricted to under 6000V as dielectric breakdowns become prevalent beyond that point. Screenshots of the elastomer sample prior and after actuation are shown in **Figure 12**.

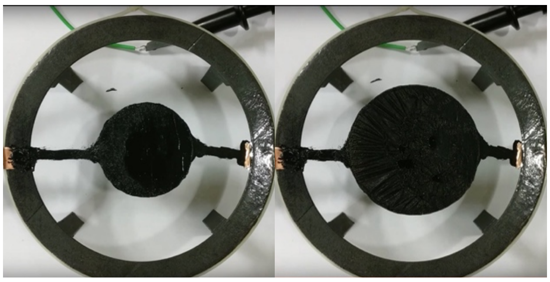

Figure 12. Strain response of the DE sample

Since Yeoh hyperelastic material model is a phenomenological model, the material constants have to be optimized to represent the phenomenon under study, which in this case is electromechanical actuation of an elastomer membrane. The optimized material constants are listed in **Table 3**.

***Table 3*: Yeoh material constants**

C10 (Pa)	7.3E+4
C20 (Pa)	0
C30 (Pa)	3.2E+5

The strain response values for these material constants are evaluated up to 5500 V in multiple load steps and the results are plotted in **Figure 13**.

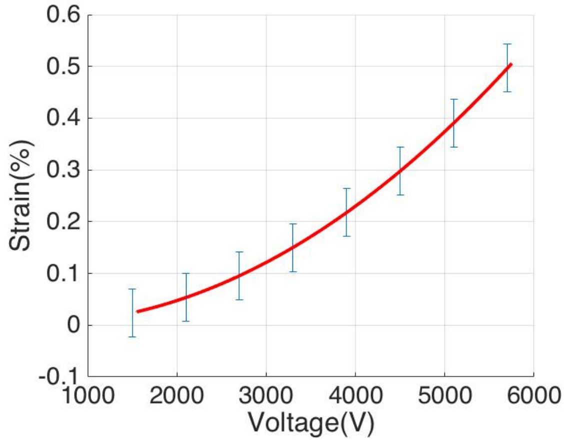

Figure 13. Finite element estimation of strain response to voltage, with error bars indicating standard deviation from experimental data

A contour plot of the element level strain intensity varying from 4.3% at the edge to 36.6% in the active region while actuated with an electric potential of 5000 V is shown in **Figure 14**.

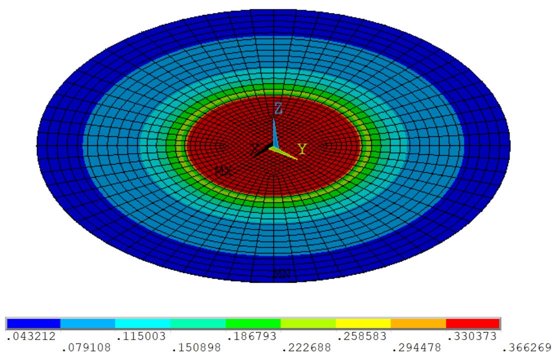

Figure 14. Strain intensity contour plot

6.2 UNIMORPH BENDER ACTUATOR

The unimorph bender actuator is iteratively evaluated for a range of electrical loads from 1500 V to 5000 V. At an electrical load of 4260 V the unimorph bender actuator is able to reach an angle of 35°, as depicted in **Figure 15**.

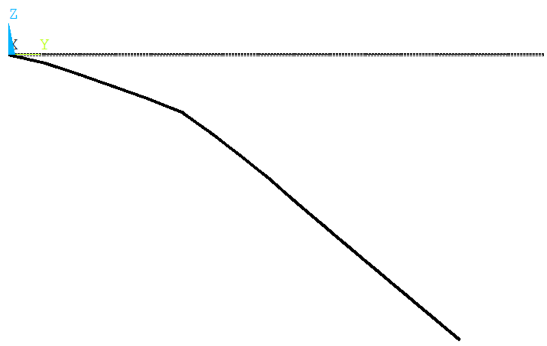

Figure 15. Side view of the deformed bender actuator and the un-deformed edge

6.3 VOLTAGE RESPONSE TO FREQUENCY

Next the sample is subjected to varying electric loads at varying frequencies. The real-time measurement of the charge and discharge time of the dielectric elastomer sample is shown in **Figure 16**. The microcontroller is programmed to consistently ramp up the upper limit of the voltage parameter every 5 cycles from a fixed lower limit of 1800V. This process is carried out for 0.5 Hz, 1 Hz, 2 Hz, 4 Hz, 8 Hz and 16 Hz. It may be noted that in all these cases the polarity is not alternating.

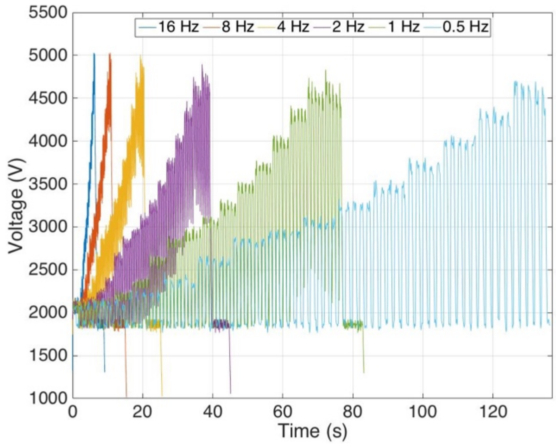

Figure 16. Voltage response to frequency

7.0 DISCUSSION

The curve fitting done to generalize the strain response to voltage for the current setup can be used to predict the strain response when incorporated into different applications. The analysis to explore the response of the elastomer to a pulsed waveform was carried forward, without adding any additional lossy circuital elements. It can be observed from voltage response obtained at higher frequencies, that due to the charge-discharge time inherent to the material and the system, the voltage values are unable to reach their programmed lower limit of 1800 V and get prematurely attenuated. The analysis was simulated to validate our SPICE capacitor modelling and produced similar results with a mean average voltage error calculated to be 314V (~ 10%). Using the strain prediction methodology, the mean average strain error can be estimated to be about 3%. This attenuation was reduced by minimizing discharging time when a resistive bleeder network was added in parallel with the elastomer (simulation) in order to achieve the target wingbeat frequency. However, this implied the bleeder contributed to a power loss during every discharge cycle of the elastomer. This can be averted if a high voltage AC circuit is implemented as the discharge will be both faster due to the negative polarity and efficient as the source will sink current instead of the bleeder. This proposed circuit is shown in **Figure 17**.

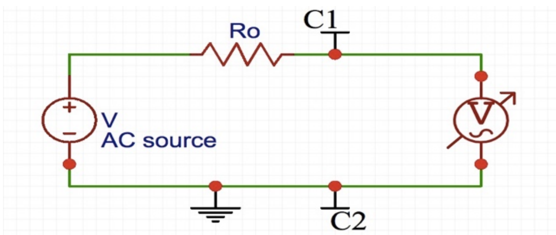

Figure 17. High voltage AC circuit

These approaches will help reach the target wingbeat frequency of 30 Hz with both DC & AC sources. Further, the validated finite element model parameters can be used to model different types of actuators driven by dielectric elastomers. This is used to design a unimorph bender actuator, to derive predictive values of stroke amplitude. Extrapolation of this unimorph structure into a bimorph, with suitable adjustments let to the model achieving the target stroke amplitude of 70°. Comfortable bending is observed both above and below the x-y plane when the dielectric elastomers sandwiching the substrate are actuated alternatively.

6.0 CONCLUSION

The underlying kinematic motions involved in flapping wing actuation was analysed and certain key target parameters governing them were isolated to evaluate the available smart materials. The evaluation resulted in the theoretical superiority of dielectric elastomers and their practicality was analysed through a series of experiments. Multiple sample of acrylic elastomers coated with compliant electrodes were subjected to a variety of electrical stimuli. Methodologies were developed to enable and complement this experimentation, by measuring the high voltage supplied and corresponding strain response observed in the elastomer. A finite element model was developed to capture the electromechanical coupling observed and extend the same for various actuator configurations. A predictive bender actuator model was developed with a length analogues to our target wing length and its ability to achieve the target stroke amplitude was tested. Further an electrical SPICE model was derived to analyse and optimize the frequency response of the system, so that the target wingbeat frequency is also achievable.

ACKNOWLEDGEMENTS

The authors would like to acknowledge Nitin Narwal, Ashish Kushwaha, Vijeth K and Nishanth Murugan for their contributions to this work. The authors would also like to thank Electrical Machines Labrotary, Shiv Nadar University for the use of their facilities. This was supported and funded by the Department of Mechanical Engineering, Shiv Nadar University.

REFERENCES

[1] D. J. Pines and F. Bohorquez, “Challenges Facing Future Micro-Air-Vehicle Development,” *J. Aircr.*, vol. 43, no. 2, pp. 290–305, Mar. 2006.
[2] L. Petricca, P. Ohlckers, and C. Grinde, “Micro- and nano-air vehicles: State of the art,” *Int. J. Aerosp. Eng.*, vol. 2011, no. Article ID 214549, p. 17 pages, 2011.
[3] S. Mukherjee and R. Ganguli, “A dragonfly inspired flapping wing actuated by electro active polymers,” *Smart Struct. Syst.*, vol. 6, no. 7, pp. 867–887, 2010.
[4] G. Sachs, “Comparison of Power Requirements: Flapping vs. Fixed Wing Vehicles,” *Aerospace*, vol. 3, no. 4, p. 31, 2016.
[5] N. Phillips and K. Knowles, “Formation of vortices and spanwise flow on an insect-like flapping wing throughout a flapping half cycle,” *Aeronaut. J.*, vol. 117, no. 1191, pp. 471–490, 2013.
[6] S. Zhang, Z. Wang, Y. Wu, and Y. Yu, “Flight dynamic coupling analysis of a bio-inspired elastic-wing aircraft,” *Aeronaut. J.*, vol. 122, no. 1250, pp. 572–597, 2018.
[7] S. P. Sane, “The aerodynamics of insect flight,” *J. Exp. Biol.*, vol. 206, no. 23, pp. 4191–4208, 2003.
[8] S. C. Burgess, C. S. Ling, A. Conn, S. Araromi, J. Wang, and R. Vaidyanathan, “Development of a novel Electro Active Polymer (EAP) actuator for driving the wings of flapping micro air vehicle,” *WIT Trans. Built Environ.*, vol. 106, pp. 207–217, 2009.
[9] X. Shen, Y. Liu, and J. Zhang, “Study of piezoelectric fiber composite actuators applied in the flapping wing,” in *2009 18th IEEE International Symposium on the Applications of Ferroelectrics*, 2009, pp. 1–4.
[10] C. P. Ellington, “The Aerodynamics of Hovering Insect Flight. I. The Quasi-Steady Analysis,” *Philos. Trans. R. Soc. Lond. B. Biol. Sci.*, vol. 305, no. 1122, pp. 1–15, 1984.
[11] A. T. Conn, C. S. Ling, and S. C. Burgess, “Biomimetic Analysis of Insect Wing Kinematics for Flapping MAVs,” *Int. J. Micro Air Veh.*, vol. 3, no. 1, pp. 1–11, 2011.
[12] C. P. Ellington, “The Aerodynamics of Hovering Insect Flight. III. Kinematics,” *Philos. Trans. R. Soc. B Biol. Sci.*, vol. 305, no. 1122, pp. 41–78, 1984.
[13] A. T. Conn, S. C. Burgess, and C. S. Ling, “Design of a parallel crank-rocker flapping mechanism for insect-inspired micro air vehicles,” *Proc. Inst. Mech. Eng. Part C J. Mech. Eng. Sci.*, vol. 221, no. 10, pp. 1211–1222, 2007.
[14] X. Cheng and M. Sun, “Wing-kinematics measurement and aerodynamics in a small insect in hovering flight,” *Sci. Rep.*, vol. 6, pp. 1–12, 2016.

[15] M. Sun and J. Tang, “Unsteady aerodynamic force generation by a model fruit fly wing in flapping motion,” *J. Exp. Biol.*, vol. 205, no. 1, pp. 55–70, 2002.
[16] Y. Zhang and M. Sun, “Wing kinematics measurement and aerodynamics of free-flight maneuvers in drone-flies,” *Acta Mech. Sin. Xuebao*, vol. 26, no. 3, pp. 371–382, 2010.
[17] J. T. Vance, D. L. Altshuler, W. B. Dickson, M. H. Dickinson, and S. P. Roberts, “Hovering Flight in the Honeybee *Apis mellifera* : Kinematic Mechanisms for Varying Aerodynamic Forces,” *Physiol. Biochem. Zool.*, vol. 87, no. 6, pp. 870–881, 2014.
[18] R. Dudley and C. P. Ellington, “Mechanics of forward flight in bumblebees: II. Quasi-steady lift and power requirements,” *J. Exp. Biol.*, vol. 148, no. 1, pp. 53–88, 1990.
[19] A. P. Willmott and C. P. Ellington, “The mechanics of flight in the hawkmoth manduca sexta: I. Kinematics of hovering and forward flight,” *J. Exp. Biol.*, vol. 200, no. Pt 21, pp. 2705–22, 1997.
[20] Q. Li, M. Zheng, T. Pan, and G. Su, “Experimental and numerical investigation on dragonfly wing and body motion during voluntary take-off,” *Sci. Rep.*, vol. 8, no. 1, pp. 1–16, 2018.
[21] R. Metzger *et al.*, *Intelligent Materials*. The Royal Society of Chemistry, 2007.
[22] S. Dynamics and G. S. Forum, “Electroactive Polymers as Artificial Muscles – Reality and Challenges Yoseph Bar-Cohen NDEAA Technologies , JPL / Caltech , Pasadena , CA,” 2001.
[23] C. Chen, Y. Tang, H. Wang, and Y. Wang, “A review of fabrication options and power electronics for flapping-wing robotic insects,” *Int. J. Adv. Robot. Syst.*, vol. 10, pp. 779–786, 2013.
[24] P. White, S. Latscha, and M. Yim, “Modeling of a Dielectric Elastomer Bender Actuator,” *Actuators*, vol. 3, no. 3, pp. 245–269, 2014.
[25] R. D. Kornbluh *et al.*, “Electroelastomers: applications of dielectric elastomer transducers for actuation, generation, and smart structures,” vol. 4698, pp. 254–270, 2002.
[26] M. Yamakita, A. Sera, N. Kamamichi, K. Asaka, and Z. W. Luo, “Integrated design of IPMC actuator/sensor,” in *Proceedings 2006 IEEE International Conference on Robotics and Automation, 2006. ICRA 2006.*, 2006, pp. 1834–1839.
[27] W. K. Wilkie *et al.*, “Low-cost piezocomposite actuator for structural control applications,” vol. 3991, pp. 323–334, 2000.
[28] K. K. Leang, Y. Shan, S. Song, and K. J. Kim, “Integrated sensing for IPMC actuators using strain gages for underwater applications,” *IEEE/ASME Trans. Mechatronics*, vol. 17, no. 2, pp. 345–355, 2012.
[29] Smart Material Corporation, “Macro Fiber Composite (MFC) Datasheet,” p. 8, 2014.
[30] J. S. Park and J. H. Kim, “Analytical development of single crystal Macro Fiber Composite actuators for active twist rotor blades,” *Smart Mater. Struct.*, vol. 14, no. 4, pp. 745–753, 2005.
[31] K. J. Yoon, S. Shin, H. C. Park, and N. S. Goo, “Design and manufacture of a lightweight piezo-composite curved actuator,” *Smart Mater. Struct.*, vol. 11, no. 1, pp. 163–168, 2002.
[32] XP Power, “Q SERIES - Isolated, Proportional DC to HV DC converters.” [Online]. Available: http://www.emcohighvoltage.com/proportional/qseries.php.
[33] R. Gupta and D. Harursampath, “Dielectric elastomers: Asymptotically-correct three-dimensional displacement field,” *Int. J. Eng. Sci.*, vol. 87, pp. 1–12, 2015.
[34] P. Brochu and Q. Pei, “Advances in dielectric elastomers for actuators and artificial muscles,” *Macromol. Rapid Commun.*, vol. 31, no. 1, pp. 10–36, 2010.
[35] R. Pelrine *et al.*, “Dielectric elastomer artificial muscle actuators: toward biomimetic motion,” vol. 4695, pp. 126–137, 2002.
[36] R. Pelrine, R. Kornbluh, and G. Kofod, “High-strain actuator materials based on dielectric elastomers,” *Adv. Mater.*, vol. 12, no. 16, pp. 1223–1225, 2000.
[37] S. M. H. and W. Y. and Q. P. and R. P. and S. Stanford, “Interpenetrating networks of elastomers exhibiting 300% electrically-induced area strain,” *Smart Mater. Struct.*, vol. 16, no. 2, p. S280, 2007.
[38] 3M, “VHB ™ Tape specialty tapes technical data,” 2014. [Online]. Available: http://multimedia.3m.com/mws/media/986695O/3m-vhb-tape-specialty-tapes.pdf.
[39] MG chemicals, “Carbon conductive grease 846 technical data sheet,” 2012. [Online]. Available: https://www.techsil.co.uk/media/pdf/TDS/MGEN00026-tds.pdf.
[40] G. Kofod, “The static actuation of dielectric elastomer actuators: How does pre-stretch improve actuation?,” *J. Phys. D. Appl. Phys.*, vol. 41, no. 21, 2008.
[41] ChengDu innovative electronic factory, “High Voltage Power Supply.” [Online]. Available: https://www.aliexpress.com/item/high-voltage-power-supply-with-10KV-12V-24V-Input-Automobile-Air-Purifier-air-cleaner/.
[42] C. Eberl, D. Gianola, and R. Thompson, “Digital Image Correlation and Tracking,” 2006. [Online]. Available: http://de.mathworks.com/matlabcentral/fileexchange/12413-digital-image-correlation-and-tracking.
[43] “Mechanical APDL Documentation,” in *ANSYS® Academic Research Mechanical documentation*

Release 19, .
[44] "SOLID226 Element Description," in *ANSYS® Academic Research Mechanical documentation, Release 19*, .
[45] M. Wissler and E. Mazza, "Modeling of a pre-strained circular actuator made of dielectric elastomers," *Sensors Actuators, A Phys.*, vol. 120, no. 1, pp. 184–192, 2005.
[46] M. Wissler and E. Mazza, "Mechanical behavior of an acrylic elastomer used in dielectric elastomer actuators," *Sensors Actuators, A Phys.*, vol. 134, no. 2, pp. 494–504, 2007.
[47] D. Armani, C. Liu, and N. Aluru, "Re-configurable fluid circuits by PDMS elastomer micromachining," in *Technical Digest. IEEE International MEMS 99 Conference. Twelfth IEEE International Conference on Micro Electro Mechanical Systems (Cat. No.99CH36291)*, 1999, pp. 222–227.